ISSN 0021-3640, JETP Letters, 2016, Vol. 104, No. 8, pp. 546–551. © Pleiades Publishing, Inc., 2016.

CONDENSED MATTER

Simulated Cu–Zr Glassy Alloys: the Impact of Composition on Icosahedral Order[1]

B. A. Klumov[a, b, c, *], R. E. Ryltsev[c, d, e], and N. M. Chtchelkatchev[c, d, f, g]

[a] *Aix-Marseille-Université, Laboratoire PIIM, CNRS, 13397 Marseille, France*

[b] *Joint Institute for High Temperatures, Russian Academy of Sciences, Moscow, 125412 Russia*

[c] *Landau Institute for Theoretical Physics, Russian Academy of Sciences, Moscow, 117940 Russia*

[d] *Institute of Metallurgy, Ural Branch, Russian Academy of Sciences, Ekaterinburg, 620016 Russia*

[e] *Ural Federal University, Ekaterinburg, 620002 Russia*

[f] *Moscow Institute of Physics and Technology (State University), Dolgoprudnyi, Moscow region, 141700 Russia*

[g] *All-Russia Research Institute of Automatics, Moscow, 127055 Russia*

**e-mail: klumov@ihed.ras.ru*

Received August 25, 2016

The structural properties of the simulated $Cu_\alpha Zr_{1-\alpha}$ glassy alloys are studied in the wide range of the copper concentration α to clarify the impact of the composition on the number density of the icosahedral clusters. Both bond orientational order parameters and Voronoi tessellation methods are used to identify these clusters. Our analysis shows that abundance of the icosahedral clusters and the chemical composition of these clusters are essentially nonmonotonic versus α and demonstrate local extrema. That qualitatively explains the existence of pinpoint compositions of high glass-forming ability observing in Cu–Zr alloys. Finally, it has been shown that Voronoi method overestimates drastically the abundance of the icosahedral clusters in comparison with the bond orientational order parameters one.

DOI: 10.1134/S0021364016200017

1. INTRODUCTION

The Cu–Zr system is in short list of binary alloys capable to form bulk-metallic glasses (BMGs) [1–3]. It has unique glass-forming ability (GFA) where compositions of BMG formation are located in narrow concentration intervals (so-called pinpoint compositions) [2, 4, 5]. One of the general ideas explaining this unusual property, strongly supported by molecular dynamics simulations, is the suggestion that local icosahedral order plays important role in GFA [6–12]. However the definition of local order contains a significant proportion of uncertainty related to the complexity of the definition of the nearest neighbors in disordered media (see, e.g., [13, 14]) and the difficulty of symmetry-classification of local clusters with a non-ideal shape. This problem makes the results of local order analysis rather challenging for practical applications.

Here, we study structural properties of the simulated $Cu_\alpha Zr_{1-\alpha}$ glassy alloys in the wide range of the copper concentration $\alpha \in (0.2,1)$ using two different methods to detect the local order: Voronoi tessellation (VT) [15] and Bond Orientational Order Parameters (BOOP) [16]. We show that a more rigorous BOOP method reveals essentially different results in comparison to those obtained by widely accepted VT method. Comparison of the BOOP and VT demonstrates that the latter significantly overestimates the number of icosahedral-like (ico-like) particles in the system. We observe that both the abundance of ico-like clusters and their chemical composition vary non-monotonically with concentration. Besides, chemical composition of ico-like clusters is found to be deviated significantly from the mixing ratio at $\alpha > 0.25$; relative lacks of copper atoms vary in the range 6–12% with a non-monotonic dependence on α.

2. METHODS

For the molecular dynamics (MD) simulations, we used the LAMMPS package [17]. The system of $N \approx 5000$ particles was simulated under periodic boundary conditions in Nose–Hoover NPT ensemble at pressure $P = 1$ atm. The MD time step was 1 fs. Initial configurations were equilibrated melts at $T = 1200$ K. The system was cooled down to $T = 300$ K with the cooling rate $\gamma = 10^{11}$ K/s. This rate was chosen to compare our results with those obtained by other authors who had used this γ value (see inset in Fig. 4).

[1] The article is published in the original.

Though in general the structure of the glass can be essentially cooling rate dependent [18–21], it is not important for this study where composition dependence of the structural properties is investigated. Interaction between alloy components is described here using a widely accepted embedded atom potential specially adopted for liquid and glassy Cu–Zr systems [22].

The BOOP method [23] is widely used in condensed matter physics to quantify the local orientational order [16, 23–25] in Lennard-Jones and hard sphere systems [26–33], complex plasmas [34–40], colloidal [41, 42] and patchy systems [43, 44], etc. The method allows us to explicitly recognize symmetry of local atomic clusters [39, 45, 46] and study their spatial distribution [47, 48].

For BOOP investigation, we define the rotational invariants of rank l of the second order q_l and third order w_l [16, 23]. The advantage of q_l and w_l is that they are uniquely determined for any polyhedron including the elements of any crystalline structure. Among the rotational invariants, q_4, q_6, w_4, and w_6 are typically the most informative ones so we use them in this work. To identify ico-like clusters we calculate the rotational invariants q_l and w_l for each atom using the fixed number of nearest neighbors ($N_{nn} = 12$). Atom whose coordinates in the space (q_4, q_6, w_4, w_6) are sufficiently close to those of the perfect structures is counted as ico-like (fcc-like, hcp-like), etc. The rotational invariants for a number of crystalline structures are shown in the table.

Rotational invariants q_l and w_l ($l = 4, 6$) of a few perfect clusters calculated via 12 nearest neighbors: icosahedron (ico), face centered cubic (fcc), and hexagonal close-packed (hcp)

Cluster type	q_4	q_6	w_4	w_6
ico	1.4×10^{-4}	0.6633	−0.1593	−0.1697
fcc	0.1909	0.5745	−0.1593	−0.0131
hcp	0.0972	0.4847	0.1340	−0.0124

3. RESULTS

Figure 1 shows two-point correlations in glassy $Cu_\alpha Zr_{1-\alpha}$ alloys at $T = 300$ K. The total radial distribution function $g(r)$ (a) and the bond angle distribution function (BADF) (b) are shown at different copper abundance α in the range of 0.2–0.95. The shoulder on the first peaks of $g(r)$ revealing the chemical-like order is clearly observed only at low α values; splitting of the second peak (which is widely used as an indicator of the glassy state and the appearance of the ico-like order in the system) occurs at moderate values $\alpha > 0.5$. Bond angle distribution function shapes at different α indicate possible presence of ico-like clusters.

Figure 2 shows the local orientational order of the glassy $Cu_\alpha Zr_{1-\alpha}$ alloys on the plane of rotational invariants $q_4 - q_6$ at few α values. Atoms distribution on the plane clearly shows the formation of Cu-centered ico-like clusters at moderate and high α values (panels b–d) and mostly disordered-like behavior (with traces of hcp-like and fcc-like clusters) at low α values (panel (a)).

To quantify the distributions in Fig. 2, we use the normalized one-dimensional probability density function over different rotational invariants $P(q_l)$ and $P(w_l)$, so that (for, e.g., q_l) $\int_{-\infty}^{\infty} P(q_l)dq_l \equiv 1$. Even more convenient is using (cumulative) distribution functions associated with the $P(q_l)$ and $P(w_l)$ [39, 45] which are defined as (by using as example the bond

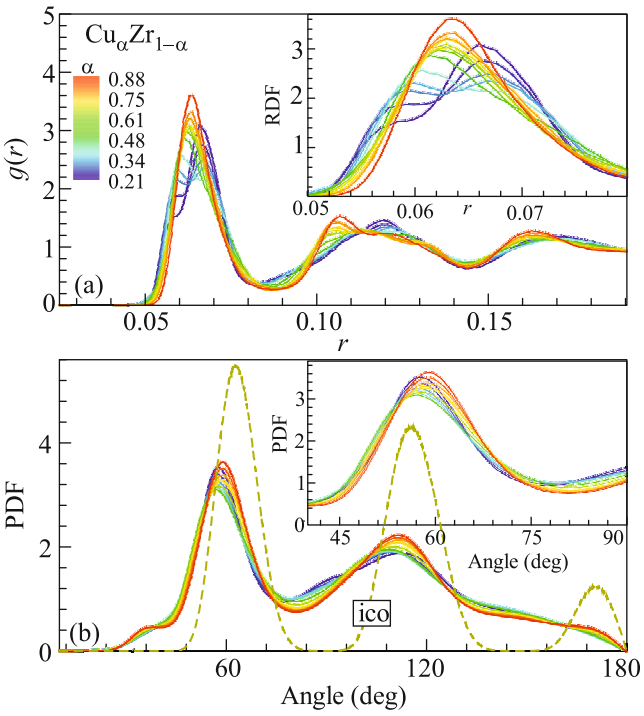

Fig. 1. (Color online) Two-point correlations in the $Cu_\alpha Zr_{1-\alpha}$ glassy system. (a) The total radial distribution function $g(r)$ and (b) the bond angle distribution function (calculated by using 12 nearest neighbors) are shown at different copper abundance α. Insets show the fine details of the first peak of these distributions. Additionally, the bond angle distribution function for the icosahedral cluster (with thermal vibrations taken into account) is plotted by the dashed line. The temperature of the system is $T = 300$ K. The cooling rate γ is 10^{11} K/s.

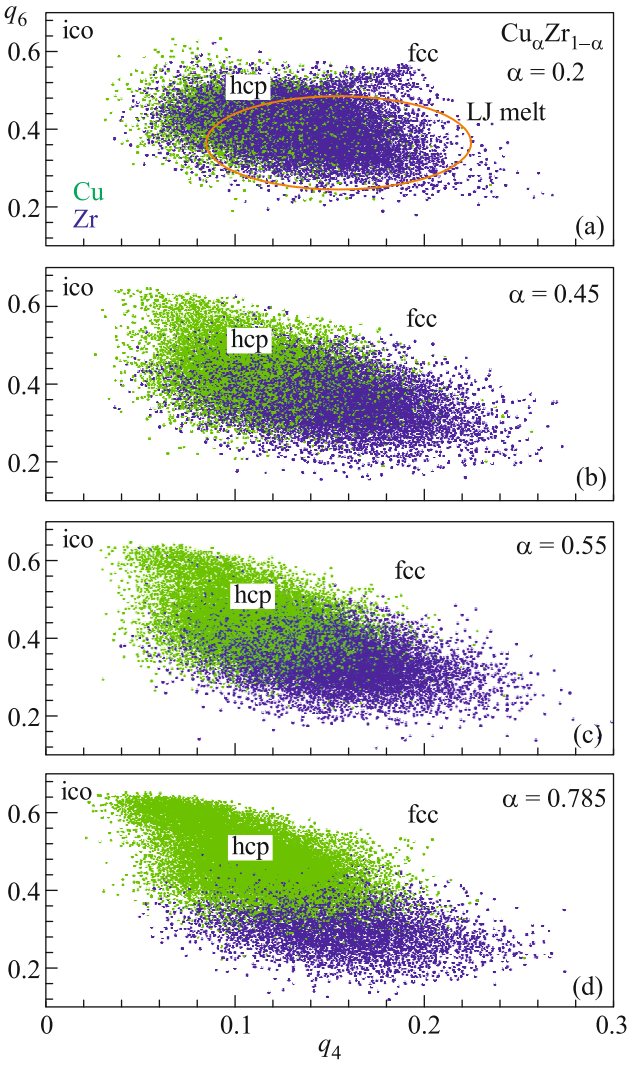

Fig. 2. (Color online) Local orientational order of the $Cu_\alpha Zr_{1-\alpha}$ system on the $q_4 - q_6$ plane at different Cu abundances α. Bond orientational order parameters (BOOP) were calculated via 12 nearest neighbors for both (green) copper and (blue) zirconium atoms to identify different close packed structures. The formation of Cu-centered ico-like clusters is clearly seen at high values of α; zirconium atoms are almost completely in a disordered liquid-like phase. Bond orientational order parameters for the perfect icosahedron, hcp and fcc clusters are also indicated for the comparison, as well as the Lennard-Jones melt distribution bounds (panel (a), orange line). The temperature of the system is $T = 300$ K.

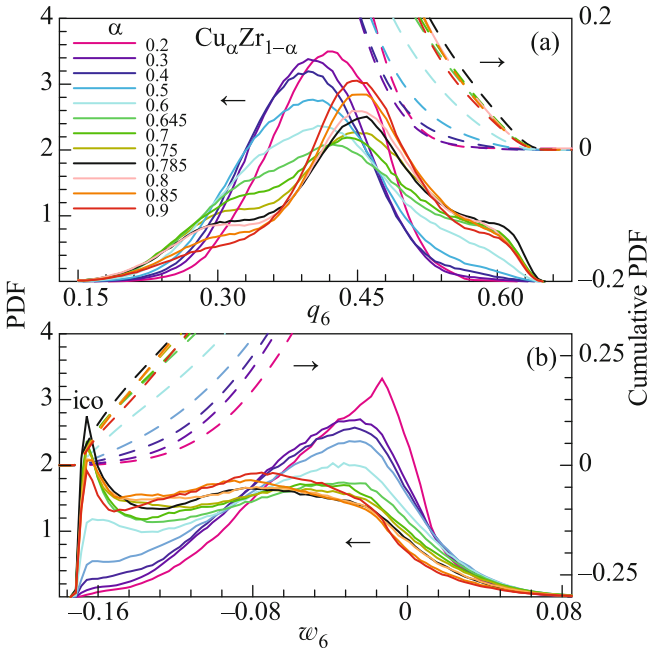

Fig. 3. (Color online) Local orientational order of the $Cu_\alpha Zr_{1-\alpha}$ system taken at $T = 300$ K: the probability distribution functions P over rotational invariants (a) q_6 and (b) w_6 at different copper abundances α. Cumulative distributions $(C_q(x) = \int_{\infty}^{x} P(q_6)dq_6$ and $C_w(x) = \int_{-\infty}^{x} P(w_6)dw_6)$ at different α values are also shown to evaluate the density of atoms with ico-like symmetry (having $q_6 > 0.6$ and $w_6 < 0.15$). An increase in α up to moderate values ($\alpha \simeq 0.5$) clearly results in an increase in ico-like clusters in the system; the increase is not monotonic then (with the maximum of the ico-like atoms at $\alpha = 0.785$ (black line)).

order parameter q_6): $C_q(x) = \int_{-\infty}^{x} P(q_6)dq_6$. Using the cumulative functions, we can find abundance (density) of any solid-like structure with a given accuracy δ_{cr}: $C_q(q^{cr} + \delta_{cr}) - C_q(q^{cr} - \delta_{cr})$, where q^{cr} is the bond order parameter for the given ideal cluster.

We note that the set of distributions P and C taken for different q_l and w_l completely describes the local orientational order in the system as an abundance of different ordered and disordered structures. Figure 3 shows how the distributions $P(q_6)$ and $P(w_6)$ and the corresponding cumulative functions C_q and C_w vary with the increase in α. Behavior of the distributions $P(q_6)$, $P(w_6)$ and $C(q_6)$, $C(w_6)$ in the vicinity of the perfect icosahedron (having $q_6^{ico} \approx 0.66$ and $w_6^{ico} \approx -0.17$ (see, table)) clearly shows nonmonotonic dependence of density of ico-like atoms on α value. For instance, at considered cooling rate ($\gamma = 10^{11}$ K/s), the maximum density of ico-like clusters occurs at $\alpha = 0.785$. To better illustrate such nonmonotonic behavior, we show in Fig. 4 the dependence of the abundance of ico-like clusters n_{ico} on Cu concentration α. A cluster is treated as ico-like one if it has order parameters $q_6 > 0.6$ and $w_6 < -0.16$. We see that $n_{ico}(\alpha)$ is essentially nonmonotonic with maximal amount of ico-like clusters within the range $0.6 < \alpha < 0.9$. Moreover, $n_{ico}(\alpha)$ demonstrates local

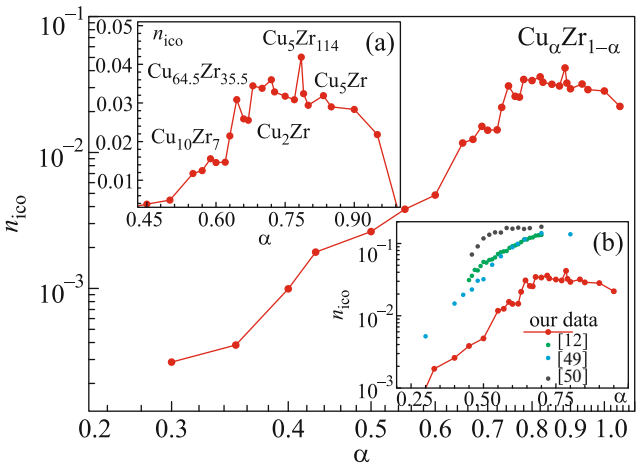

Fig. 4. (Color online) Simulated $Cu_\alpha Zr_{1-\alpha}$ alloy at $T = 300$ K. Main frame: abundance of ico-like clusters n_{ico} (calculated via cumulative functions $C_q(q_6)$ and $C_w(w_6)$ presented in Fig. 3) versus copper abundance α. Non-monotonic behavior of the ico-like cluster density is seen at $\alpha \geq 0.5$. Inset (a) shows the fine details of $n_{ico}(\alpha)$ dependence in the range $\alpha > 0.45$. Inset (b) shows comparison of our $n_{ico}(\alpha)$ dependence with those obtained by other authors [12, 49, 50].

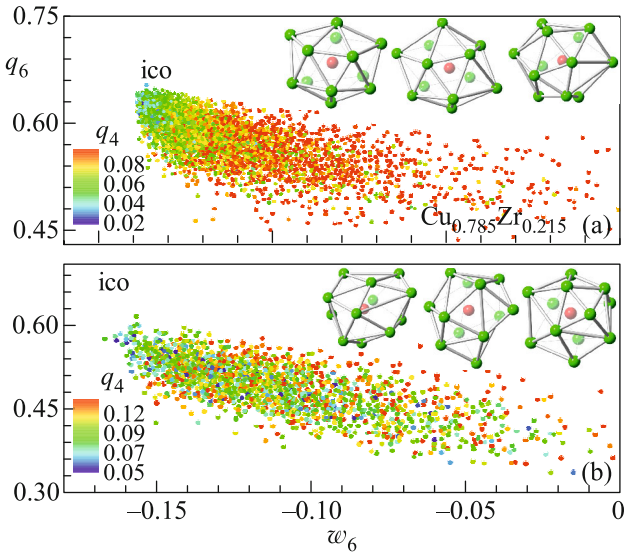

Fig. 5. (Color online) Alloy $Cu_{0.785}Zr_{0.215}$ at $T = 300$ K. Comparison of the Voronoi and BOOP methods for the ico-like cluster identification. The distribution of the particles counted as (a) full icosahedra (i.e., having Voronoi index $\langle 0,0,12,0\rangle$) and (b) distorted icosahedra (having Voronoi index $\langle 0,2,8,2\rangle$) on the plane of rotational invariants $w_6 - q_6$. Particles are color-coded via q_4 value. Insets show corresponding ico-like clusters (with red-colored central atom).

extrema located at stoichiometry compounds of a few Cu–Zr intermetallic compounds as well at the BMG composition $Cu_{0.645}Zr_{0.355}$. The presence of such extrema correlates with the existence of pinpoint compositions of BMG formation in real Cu–Zr alloys. Indeed, the ranges of local $n_{ico}(\alpha)$ maxima are expected to correspond to high GFA compositions. The very fact that simple EAM model potential can describe such non-trivial behavior (at least qualitatively) is the important result. Moreover, the maximum at $Cu_{0.645}Zr_{0.355}$ composition exactly corresponds to one of the pinpoint composition of BMG formation. So even the quantitative agreement with experimental data takes place.

In the right inset of Fig. 4, we also show the comparison of our data with those obtained in [12, 49, 50]. As is seen in this figure, our $n_{ico}(\alpha)$ curve demonstrates qualitatively the same behavior as those obtained by other authors. However, quantitatively, our n_{ico} values are much lower than those presented in [12, 49, 50]. The main reason for such deviation is the difference of methods used to determine ico-like clusters. Our results were obtained by BOOP method but the others by VT one. The latter is the most accepted method to study short- and medium-range order of metallic alloys [51, 52]. The main point of the method is dividing the space into polyhedra which faces are planes bisecting the lines connecting each particle with its nearest neighbors. The symmetry of polyhedra is determined by Voronoi indices like $\langle n_3, n_4, n_5, n_6\rangle$ where n_i is the number of i-edged faces. Voronoi index is a topologically stable characteristic that is not sensitive to deformation of the clusters. For example, any polyhedron with the index $\langle 0,0,12,0\rangle$ is treated as an icosahedron regardless of its distortion degree. That can cause the false determination of clusters structure and their abundances. That can also be the reason for the absence of local extremal in $n_{ico}(\alpha)$ curves obtained by VT method.

To show that, we compare the results obtained by both methods for ico-like clusters in $Cu_{0.785}Zr_{0.215}$ alloy. Top panel in Fig. 5 presents the distribution of particles counted by VT method as full icosahedra, i.e., the particles with the Voronoi index $\langle 0,0,12,0\rangle$ on the plane of rotational invariants $w_6 - q_6$. Bottom panel in Fig. 5 shows the same distribution taken for the clusters with Voronoi index $\langle 0,2,8,2\rangle$ usually treated as "distorted icosahedra." Particles are color-coded via q_4 value. From the data presented in panel (a), we see that significant part of particles have $q_6 < 0.6$ and $w_6 > 0.16$; i.e., these particles cannot be counted as ico-like particles if we use BOOP method. Although these clusters look like strongly distorted icosahedrons, some of the clusters are actually distorted hcp-like and fcc-like clusters, not ico-like ones. As to particles shown in bottom panel (which are counted by Voronoi method as distorted icosahedrons), nearly all

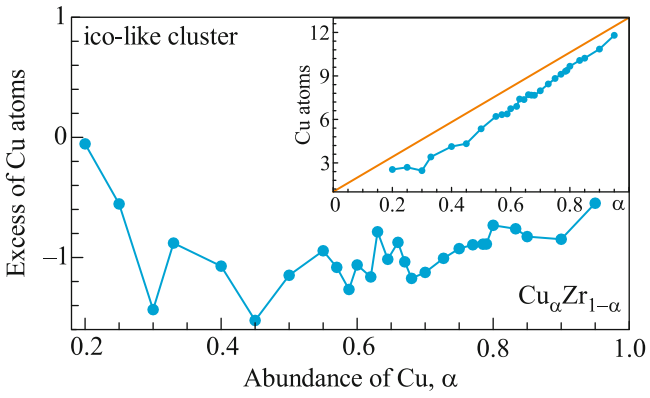

Fig. 6. (Color online) Mean chemical composition of the ico-like clusters observed in the simulated $Cu_\alpha Zr_{1-\alpha}$ system (taken at $T = 300$ K). Presented is the mean excess of Cu atoms in the cluster (with the α value being subtracted) versus copper abundance α. Inset shows how the mean number of Cu atoms in the clusters deviates from the mixing ratio α (orange line). Lack of Cu atoms in the ico-like cluster occurs at $\alpha > 0.2$; the lack nonmonotonically depends on the α value.

of them are quite far from even distorted icosahedron; these particles have q_6 and w_6 values which are typical for intermediate phase in between icosahedral and hcp/fcc type of symmetry.

Besides the symmetry of local clusters, their chemical composition may be important to understand structure of multicomponent glasses [12, 53]. In Fig. 6, we present the mean chemical composition $N_{Cu}(\alpha)$ of the ico-like clusters. In fact, the mean excess concentration of Cu atoms in the cluster $\delta N_{Cu}(\alpha) \equiv N_{Cu}(\alpha) - \alpha$ is plotted versus α. The inset shows how the value $N_{Cu}(\alpha)$ deviates from the mixing ratio α. Lack of Cu atoms in the ico-like cluster occurs at $\alpha > 0.2$; the lack nonmonotonically depends on the α value. The minimum value of $\delta N_{Cu}(\alpha)$ occurs at $\alpha = 0.45$ with $\delta N_{Cu}(\alpha)/N_{cl} \approx -0.12$, where $N_{cl} = 13$ is the number of atoms in the cluster. In the range of interest of copper abundance ($\alpha \in 0.6$–0.8), values of $\delta N_{Cu}(\alpha)/N_{cl} \simeq -0.08$. It is also seen that local extrema of $\delta N_{Cu}(\alpha)$ curve occur at the same $\alpha = 0.645, 0.785$ as those on $n_{ico}(\alpha)$ dependence. That means that abundance of ico-like clusters and their chemical composition are correlated.

4. CONCLUSIONS

To conclude we investigated the local orientational order of the simulated $Cu_\alpha Zr_{1-\alpha}$ metallic glass in fine detail by using bond order parameter method. We show that abundance of the ico-like clusters and the chemical composition of these clusters are essentially nonmonotonic versus α and demonstrate local extrema. That qualitatively explains the existence of pinpoint concentrations of high glass-forming ability observing in Cu–Zr alloys. Finally, it has been shown that VT method overestimates drastically the abundance of the ico-like clusters in comparison with the BOOP one.

Molecular dynamics simulations was supported by the Russian Science Foundation (RSF) (project no. 14-13-00676). Structural analysis was supported by RSF (project no. 14-12-01185). Program codes for local orientational order analysis were developed within the frames of the grant RSF 14-50-00124. The work of B.A.K. was supported by the A*MIDEX grant (no. ANR-11-IDEX-0001-02) funded by the French Government "Investissements d'Avenir" program managed by the French National Research Agency (ANR). The Institute of Metallurgy is grateful to the Ural Branch, Russian Academy of Sciences for access to the URAN computer cluster.

REFERENCES

1. D. Xu, B. Lohwongwatana, G. Duan, W. L. Johnson, and C. Garland, Acta Mater. **52**, 2621 (2004).
2. D. Wang, Y. Li, B. B. Sun, M. L Sui, K. Lu, and E. Ma, Appl. Phys. Lett. **84**, 4029 (2004).
3. W. H. Wang, J. J. Lewandowski, and A. L. Greer, J. Mater. Res. **20**, 2307 (2005).
4. Y. Li, Q. Guo, J. A. Kalb, and C.V. Thompson, Science **322**, 1816 (2008).
5. L. Yang, G. Q. Guo, L.Y. Chen, C. L. Huang, T. Ge, D. Chen, P. K. Liaw, K. Saksl, Y. Ren, Q. S. Zeng, B. LaQua, F. G. Chen, and J. Z. Jiang, Phys. Rev. Lett. **109**, 105502 (2012).
6. M. Li, C. Z. Wang, S. G. Hao, M. J. Kramer, and K. M. Ho, Phys. Rev. B **80**, 184201 (2009).
7. H. L. Peng, M. Z. Li, W. H. Wang, C.-Z. Wang, and K. M. Ho, Appl. Phys. Lett. **96**, 021901 (2010).
8. R. Soklaski, Z. Nussinov, Z. Markow, K. F. Kelton, and L. Yang, Phys. Rev. B **87**, 184203 (2013).
9. Z. W. Wu, M. Z. Li, W. H. Wang, and K. X. Liu, Phys. Rev. B **88**, 054202 (2013).
10. D. D. Wen, P. Peng, Y. Q. Jiang, and R. S. Liu, J. Non-Cryst. Solids **378**, 61 (2013).
11. L. L. Meng, L. Wang, S. H. Wang, and Y. Qi, Phys. Chem. Liq. **53**, 348 (2015).
12. D. Wang, S.-J. Zhao, and L.-M. Liu, J. Phys. Chem. A **119**, 806 (2015).
13. J. A. van Meel, L. Filion, C. Valeriani, and D. Frenkel, J. Chem. Phys. **136**, 234107 (2012).
14. A. Malins, S.R. Williams, J. Eggers, and C. P. Royall, J. Chem. Phys. **139**, 234506 (2013).
15. F. Aurenhammer, ACM Comput. Surv. **23**, 345 (1991).
16. P. J. Steinhardt, D. R. Nelson, and M. Ronchetti, Phys. Rev. Lett. **47**, 1297 (1981).
17. S. Plimpton, J. Comput. Phys. **117**, 1 (1995).
18. K. Vollmayr, W. Kob, and K. Binder, J. Chem. Phys. **105**, 4714 (1996).

19. F. Zhang, M. I. Mendelev, Y. Zhang, C.-Z. Wang, M. J. Kramer, and K.-M. Ho, Appl. Phys. Lett. **104**, 061905 (2014).
20. Y.-J. Hu, D.-D. Wen, Y.-Q. Jiang, Y.-H. Deng, and P. Peng, T. Nonferr. Metal. Soc. **25**, 533 (2015).
21. R. E. Ryltsev, B. A. Klumov, N. M. Chtchelkatchev, and R. Y. Shunyaev, J. Chem. Phys. **145**, 034506 (2016).
22. M. I. Mendelev, M. J. Kramer, R. T. Ott, D. J. Sordelet, D. Yagodin, and P. Popel, Philos. Mag. **89**, 967 (2009).
23. P. J. Steinhardt, D. R. Nelson, and M. Ronchetti, Phys. Rev. B **28**, 784 (1983).
24. A. C. Mitus and A. Z. Patashinskii, Phys. Lett. A **87**, 179 (1982).
25. T. M. Truskett, S. Torquato, and P. G. Debenedetti, Phys. Rev. E **62**, 993 (2000).
26. J. R. Errington, P. G. Debenedetti, and S. Torquato, J. Chem. Phys. **118**, 2256 (2003).
27. M. D. Rintoul and S. Torquato, J. Chem. Phys. **105**, 9258 (1996).
28. V. Luchnikov, A. Gervois, P. Richard, L. Oger, and J. P. Troadec, J. Mol. Liq. **96–97**, 185 (2002).
29. Y. Jin and H. A. Makse, Physica A **389**, 5362 (2010).
30. B. A. Klumov, JETP Lett. **97**, 327 (2013).
31. B. A. Klumov, JETP Lett. **98**, 259 (2013).
32. V. Baranau and U. Tallarek, Soft Matter **10**, 3826 (2014).
33. B. A. Klumov, Y. Jin, and H. A. Makse, J. Phys. Chem. B **118**, 10761 (2014).
34. G. E. Morfill, A. V. Ivlev, S. A. Khrapak, B. A. Klumov, M. Rubin-Zuzic, U. Konopka, and H. M. Thomas, Contrib. Plasm. Phys. **44**, 450 (2004).
35. M. Rubin-Zuzic, G. E. Morfill, A.V. Ivlev, R. Pompl, B. A. Klumov, W. Bunk, H. M. Thomas, H. Rothermel, O. Havnes, and A. Fouquet, Nat. Phys. **2**, 181 (2006).
36. B. A. Klumov and G. E. Morfill, J. Exp. Theor. Phys. **107**, 908 (2008).
37. B. A. Klumov and G. E. Morfill, JETP Lett. **90**, 444 (2009).
38. B. Klumov, P. Huber, S. Vladimirov, H. Thomas, A. Ivlev, G. Morfill, V. Fortov, A. Lipaev, and V. Molotkov, Plasma Phys. Contr. Fusion. **51**, 124028 (2009).
39. B.A. Klumov, Phys. Usp. **53**, 1053 (2010).
40. S. A. Khrapak, B. A. Klumov, P. Huber, V. I. Molotkov, A. M. Lipaev, V. N. Naumkin, A. V. Ivlev, H. M. Thomas, M. Schwabe, G. E.Morfill, O. F. Petrov, V. E. Fortov, Yu. Malentschenko, and S. Volkov, Phys. Rev. E **85**, 066407 (2012).
41. U. Gasser, E. R. Weeks, A. Schofield, P. N. Pusey, and D. A. Weitz, Science **292**, 258 (2001),
42. T. Kawasaki and H. Tanaka, Proc. Natl. Acad. Sci. **107**, 14036 (2010).
43. O. A. Vasilyev, B. A. Klumov, and A. V. Tkachenko, Phys. Rev. E **88**, 012302 (2013).
44. O. A. Vasilyev, B. A. Klumov, and A. V. Tkachenko, Phys. Rev. E **92**, 012308 (2015).
45. B. A. Klumov, S. A. Khrapak, and G. E. Morfill, Phys. Rev. B **83**, 184105 (2011).
46. A. Hirata, L. J. Kang, T. Fujita, B. Klumov, K. Matsue, M. Kotani, A.R. Yavari, and M.W. Chen, Science **341**, 376 (2013).
47. R. E. Ryltsev and N. M. Chtchelkatchev, Phys. Rev. E **88**, 052101 (2013).
48. R. Ryltsev, B. Klumov, and N. Chtchelkachev, Soft. Matter **11**, 6991 (2015).
49. L. Ward, D. Miracle, W. Windl, O. N. Senkov, and K. Flores, Phys. Rev. B **88**, 134205 (2013).
50. K. N. Lad, J. Non-Cryst. Solids **404**, 55 (2014).
51. J. L. Finney, Proc. R. Soc. London, Ser. A **319**, 479 (1970).
52. Y. Q. Cheng and E. Ma, Prog. Mater. Sci. **56**, 379 (2011).
53. A. Malins, J. Eggers, C. P. Royall, S. R. Williams, and H. Tanaka, J. Chem. Phys. **138**, 12 (2013).